Journal of Power Sources 196 (2011) 3426–3432

Contents lists available at ScienceDirect

Journal of Power Sources

journal homepage: www.elsevier.com/locate/jpowsour

Fe^{II}/Fe^{III} mixed-valence state induced by Li-insertion into the metal-organic-framework Mil53(Fe): A DFT+U study

C. Combelles, M. Ben Yahia, L. Pedesseau, M.-L. Doublet*

Institut Charles GERHARDT – CNRS and Université Montpellier 2, Place Eugène Bataillon, 34095 Montpellier, France

ARTICLE INFO

Article history:
Received 31 March 2010
Received in revised form 24 August 2010
Accepted 25 August 2010
Available online 24 September 2010

Keywords:
Lithium-ion batteries
First-principles DFT calculations
Redox mechanisms
Mixedvalence
State

ABSTRACT

The iron-based metal-organic-framework MIL53(Fe) has recently been tested as a cathode materials for Li-Ion batteries, leading to promising cycling life and rate capability. Despite a poor capacity of 70 mAh g^{-1} associated with the exchange of almost 0.5Li/Fe, this result is the first evidence of a reversible lithium insertion never observed in a MOF system. In the present study, the MIL53(Fe) redox mechanism is investigated through first-principles DFT+U calculations. The results show that MIL53(Fe) is a weak antiferromagnetic charge transfer insulator at $T = 0$ K, with iron ions in the high-spin $S = 5/2$ state. Its reactivity vs elemental lithium is then investigated as a function of lithium composition and distribution over the most probable Li-sites of the MOF structure. The redox mechanism is fully interpreted as a two-step insertion/conversion mechanism, associated with the stabilization of the Fe^{3+}/Fe^{2+} mixed-valence state prior to the complete decomposition of the inorganic–organic interactions within the porous MOF architecture.

Published by Elsevier B.V.

1. Introduction

The search for new electrode materials for Li-ion batteries has attracted a lot of attention over the past decade. For positive electrodes, the functionalization of the oxygen ligands by a σ-acceptor ligand such as PO_4 in the $LiFePO_4$ has opened new routes for tuning the electrochemical potentials of transition metal oxides (TM-O) [1–3]. In transition metal phosphates, the effect of the σ-acceptor ligand is to polarize the electron density towards the internal PO_4 sphere and to decrease the metal to ligand interaction. This induces a significant lowering in energy of the (metallic-like) redox band of the whole system, and consequently an increase of its electrochemical potential versus lithium. However, another effect of the PO_4 acceptor ligand is to electronically isolate the transition metal (redox centre of the electrochemical reaction) thus preventing from metal to ligand back-donation mechanisms upon the reduction [4]. Following that line, we checked the opportunity to use π-acceptor ligands such as the benzene-1,4-dicarboxylate BDC ($O_2C–C_6H_4–CO_2$) to take advantage of the π-conjugated system of this organic ring and to favor the metal to ligand back-donation mechanism. In molecular coordination chemistry such a metal to ligand back-donation is known to release the strong electron correlation onto the metallic 3*d* orbitals. This study allowed us to show the first reversible lithium insertion in a metal-organic-framework (MOF) architecture [5]. These porous materials contain inorganic and organic networks and are commonly used in sensing, catalysis, ion exchange, separations or gas storage [6–12]. Among them, the MIL53(Fe) of formulation $Fe(OH)_{0.8}F_{0.2}(BDC)$ is the most promising one regarding its Li-reactivity versus elemental lithium [5]. It shows interesting performances, such as good cycling life and rate capability but a disappointing capacity of 70 mAh g^{-1} associated with the exchange of ∼0.6Li/Fe. In order to improve the total capacity of these MOFs, a mandatory step is now to understand the redox mechanism involved in these materials. The aim of this work is then to find out the origin of the limited capacity of MIL53(Fe) electrode, by means of first-principles density functional theory (DFT) calculations and local chemical bond analyses. Computational methods such as DFT have already proven to be powerful in predicting the thermodynamic, structural and electronic properties of a wide series of solids. It is also well admitted that variants of the standard DFT such as self-interaction corrected DFT+U [13–15] methods are required to properly account for the electron correlation in dense transition metal and rare earth-based systems [16]. This approach allows for a better treatment of ground state properties such as local magnetization and charge/spin ordering, by introducing an effective on-site Hubbard-like parameter U_{eff} on the subset of correlated states, *i.e.* in the present case the Fe(3*d*)-orbitals. In a previous study [4], we have investigated the structural, electronic and magnetic properties of the neutral MIL53(Fe) from the DFT limit ($U_{eff} = 0$) to the strongly correlated limit ($U_{eff} = 9$ eV) within the GGA+U formalism. In this study, a value of $U_{eff} = 5$ eV was determined as the pertinent parameter to reproduce the lat-

* Corresponding author. Tel.: +33 467143681; fax: +33 467144839.
E-mail address: doublet@univ-montp2.fr (M.-L. Doublet).

0378-7753/$ – see front matter. Published by Elsevier B.V.
doi:10.1016/j.jpowsour.2010.08.065

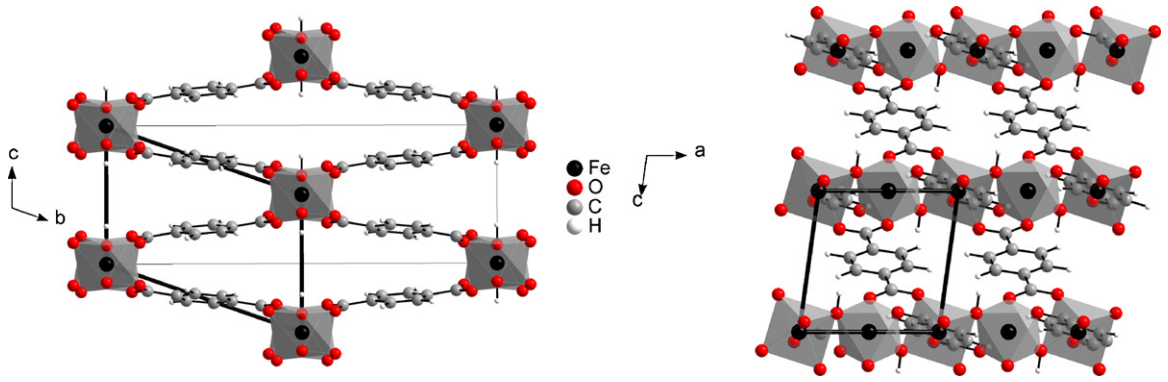

Fig. 1. Crystal structure of the MIL53(Fe) described in the $C_{2/c}$ (grey) and P_{-1} (black) unit cells with hydroxyl bridging ligands (OH) along the inorganic chains.

tice parameters and the local Fe–O bond lengths of the system, as well as the room-temperature paramagnetic behavior and the magnetic and Mossbauer signatures of this system. In the present work, we investigate the electrochemical properties of the MIL53(Fe) towards lithium, using the U_{eff} parameter previously defined. To elucidate the redox mechanism involved in that system, we consider the most probable lithium sites among the numerous ones available in such open structures, and we use local chemical bond analyses to discuss the results of the DFT+U calculations.

2. Computational details

All calculations were performed using the plane-wave density functional theory (DFT) code from the Vienna *ab initio* Simulation Package (VASP) [18,19] within the generalized gradient approximation of Perdew-Burke-Ernzerhof (GGA-PBE) [20] for the exchange and correlation potentials and the GGA+U formalism of Dudarev et al. [15] with U_{eff} = 5 eV (U = 4 eV; J = 1 eV). Note that this U_{eff} value is very close to the one usually chosen in iron oxides and iron phosphates to compute the redox potentials associated with Li insertion (*i.e.* 4.6–4.9 eV) [21]. The electron wave functions were described in the projected augmented wave formalism (PAW) [22] and a real-space projection was further used for the total wave function analyses. The plane wave energy cutoff was set to 600 eV and the Brillouin zone integration was done in a k-point grid distributed as uniformly as possible, using a $5 \times 3 \times 5$ Monkhorst-Pack mesh (38 irreducible k-points) for structural relaxations and a $7 \times 5 \times 7$ (123 irreducible k-points) for density of states and band structure analyses, in the P_{-1} primitive cell. The ionic convergence was done with respect to both the atomic forces ($<3 \times 10^{-3}$ Å eV^{-1}) and the energies ($<10^{-5}$ eV).

3. Results

3.1. MIL53(Fe) ground state

The MIL53(Fe) crystallizes in the monoclinic $C_{2/c}$ space group (no. 15) with unit cell parameters a = 6.882 Å, b = 21.249 Å, c = 6.763 Å and γ = 114.6. As shown in Fig. 1, it consists in chains of FeO_6 (or FeO_5F) pseudo-octahedra along the a direction of the crystal lattice. These molecular units are connected along the chain through a hydroxyl (OH) or a fluorine (F) bridging ligand and between the chains through the organic BDC-linkers. The fluorine atoms are statistically distributed along the chains on appreciatively one over four iron ions, leading to the general formulation $Fe(OH)_{0.8}F_{0.2}(O_2C–C_6H_4–CO_2)$ and to a large unit cell made of 75 atoms. Using first-principles methods, such a unit cell leads to very time- and disk-consuming calculations, in particular when full structural relaxations are required. However, in order to reduce the computational time, a symmetry lowering from the $C_{2/c}$ to the P_{-1} space group can be used to build a twice smaller unit cell (36 atoms) in which all fluorine atoms are removed and replaced by hydroxyl groups, *i.e.* FeOH(BDC). The P_{-1} unit cell now consists in one chain built on two independent iron atoms, namely Fe(1) and Fe(2). Note that this approximation is justified by the fact that the fluorine-free MIL53(Fe) compound has also been electrochemically tested. Compared to the fluorinated compound, it shows a slightly smaller capacity whose origin will be discussed in the last section.

As shown in Table 1, the MIL53(Fe) experimental and computed parameters are in very good agreement with a relative error <2%. Focusing on the local magnetic moment of the iron ions, a value of 4.3μ_B is obtained which agrees the high-spin configuration of the Fe^{3+} (d^5) ions and the Mossbauer signature of the MIL53(Fe) [5]. Note that the magnetization obtained in first-principles calculations is always lower than the experimental one (*i.e.* 5.92μ_B for HS-Fe^{3+}) due to the contribution of the oxygen orbitals and to the absence of orbital moment contribution. The different magnetic structures arising from the different spin arrangements along the chains have then be considered. They correspond to ferromagnetic (FM) or antiferromagnetic (AF) interactions between adjacent iron ions along the chains. It should be noted here that within the conventional $C_{2/c}$ unit cell (consisting in two chains and 4 Fe) the inter-chain magnetic interactions can also be considered, and were shown to be negligible [4,17]. As shown in Table 1 the energy difference between the AF and FM structures ($\Delta E = E(AF) - E(FM)$) is 44 meV per formula unit, showing that the AF structure is slightly favored compared to the FM one by $<2k_BT$. Given the error of the method, this is consistent with both the RT paramagnetic behavior and the paramagnetic to antiferromagnetic transition observed at 7 K for the MIL53(Fe).

The total and projected density of states (DOS) of the MIL53(Fe) starting phase are presented in Fig. 2a for the most stable AF struc-

Table 1
Experimental and computed lattice parameters, relative errors (in parenthesis), iron local magnetic moment μ_B(Fe) and relative energy of the FM and AF structures (AE per formula unit), computed with GGA+U (U_{eff} = 5 eV) for the MIL53(Fe) compound.

MIL53 (Fe)	a (Å)	b (Å)	c (Å)	μ_B (Fe) (μ_B)	ΔE/FU (meV)
Exp.	6.882	11.150	6.763	5.92	AF (T = 0 K)
AF	7.022 (2.03%)	11.230 (0.72%)	6.892 (1.90%)	4.33	0
FM	6.996 (1.65%)	11.234 (0.75%)	6.839 (1.12%)	4.36	44

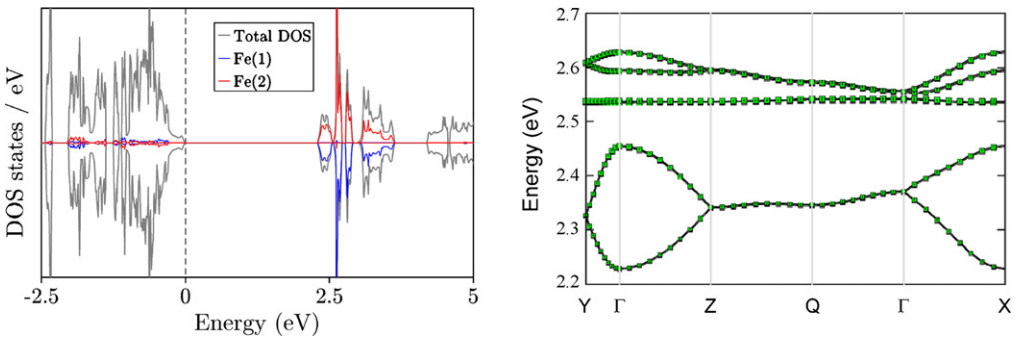

Fig. 2. (a) Total density of state and its projection over the Fe(1), Fe(2) and BDC atomic levels and (b) electronic band structure above the Fermi level (redox band) for the MIL53(Fe) compound computed in the P_{-1} unit cell using the GGA-U formalism with U_{eff} = 5 eV, and the Γ(0, 0, 0), X(1/2, 0, 0), Y(0, 1/2, 0), Z(0, 0, 1/2), Q(0, 1/2, 1/2) k-point projections in the reciprocal lattice.

ture computed in the primitive (P_{-1}) unit cell. As shown on that picture, the low-lying band (below the Fermi level) is mainly centered on the orbitals of the organic linker (BDC) while the high-lying band (above the Fermi level) shows both metallic and ligand contributions, the former being significantly larger than the latter. This suggests that MIL53(Fe) is a charge transfer insulator at T = 0 K with an energy band gap of E_g = 2.45 eV. While the DFT formalism is well-known to underestimate the band gap of insulators and semiconductors, the DFT+U formalism is expected to significantly improve it, provided that the proper ground state is reached by the self-consistent calculations [23]. Attempts to measure the MIL53(Fe) experimental gap have led to a value of 2.4 eV [24]. Although caution is required for such direct comparison, this value is very close to our GGA+U calculations, using U_{eff} = 5 eV.

Before investigating the electrochemical properties of the MIL53(Fe) system, it is interesting to pay attention on its redox band. As mentioned above, this band (see Fig. 2b) exhibits both a metallic (Fe) and a ligand (BDC) contribution. This suggests that a Fe → BDC back-donation mechanism could occur upon lithiation, given that an efficient overlap exists between the metallic 3d-orbitals and the BDC π-like orbitals. This mechanism should allow the transition metal to minimize the strong electron repulsion of its 3d-electrons by transferring a certain amount of the additional electrons coming from lithium insertion into the MIL53(Fe) to the π-delocalized orbitals of the organic linker. As shown in Fig. 2b, the redox band is significantly dispersive along the $\Gamma \rightarrow X$, $\Gamma \rightarrow Y$ and $\Gamma \rightarrow Z$ directions of the reciprocal lattice. This shows that the metallic 3d-orbitals significantly overlap with the BDC ligands and that some electron delocalization could take place both along the inorganic chains and between the chains through the organic linkers. The MIL53(Fe) should thus exhibit a two-dimensional electronic character as soon as the electrochemical reduction begins. It is worth noting however, that the electronic delocalization along the chains may only occur in the FM state since, as illustrated in Fig. 3, no electron hoping is possible in the AF state, even when electrons are added to the system.

3.2. MIL53(Fe) redox properties

To investigate the redox properties of the MIL53(Fe), it is interesting to decouple the electronic and ionic effects of the electrochemical reaction. A purely electronic reduction was then considered first, by simply adding electrons to the neutral system. Then lithium atoms were included into the MIL53(Fe) porous structure to quantify the ionic effect on the complete electrochemical reduction and to compare the computed open-circuit voltages of the system to experiments. Note that the electronic reduction allows not only to access intermediate reduction rates (since a fraction of electron can be added to the system) but also to model a

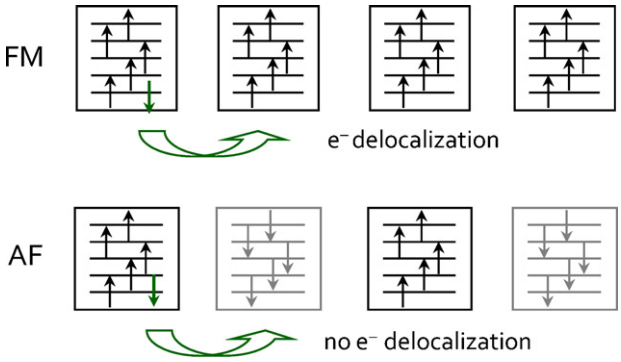

Fig. 3. Illustration of the electronic localization/delocalization of one extra-electron along a chain of Fe^{3+} ions in the high-spin state in case of (a) antiferromagnetic (AF) and (b) ferromagnetic (FM) interactions between next-nearest neighbors.

statistical distribution of lithium which is likely to occur in such porous materials with a large number of crystallographically independent sites for lithium insertion. In Fig. 4, we have reported the evolution of the Fe(1) and Fe(2) local magnetic moments as a function of the number of electron(s) added to the system. Interestingly, the addition of n electrons to the MIL53(Fe) system results in different responses of the AF and FM magnetic structures. As previously expected for the AF structure, no electronic delocalization occurs along the inorganic chains when the system is electronically reduced. As a consequence, the exceeding charge localizes on one every $1/n$ iron, leading to the stabilization of one Fe^{2+} over $1/n$ Fe^{3+} ions along the chains. Further structural relaxations per-

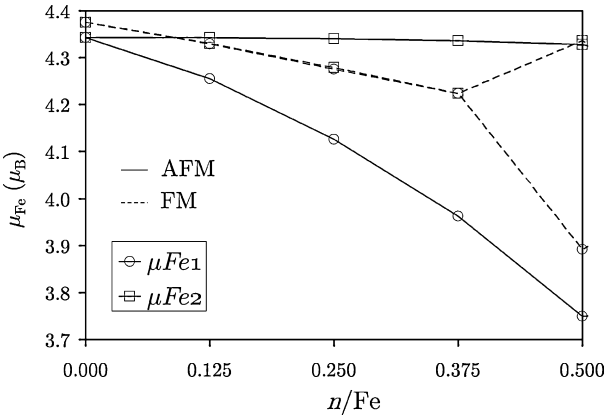

Fig. 4. Variation of the local magnetic moment of Fe(1) and Fe(2) as a function of the number of electrons added to the neutral MIL53(Fe) system (n/Fe) and computed in the P_{-1} unit cell using the GGA-U formalism with U_{eff} = 5 eV for both the AF and FM structures.

formed at each step of the reduction clearly show a local distortion around the Fe^{2+} ions, in perfect agreement with the Fe–O bond elongation resulting from the filling of Fe–O antibonding electronic levels. Note that the equatorial Fe–O(C) bonds are much more sensitive to the electronic reduction than the Fe–O(H) apical bonds, due to their larger contribution to the electronic levels involved in the reduction process. The equatorial bonds are found to become nearly equivalent for the Fe^{2+}, leading to a pseudo-D_{4h} symmetry (4×2.205 Å), while they differ by 0.1 Å for the Fe^{3+} ion (2×2.012 Å, 2×2.112 Å). The fact that the Fe–O(H) apical bonds are not significantly affected by the electronic reduction is consistent with the small variation of the intra-chain *a* parameter which increases from 7.022 to 7.192 Å when *n*/Fe is increased from 0 to 0.5. In the FM state, the situation is very different: the additional charge first delocalizes homogeneously over the two iron ions, leading to a fractional $Fe^{(3-n/2)+}$ oxidation state and to homogeneously lowered magnetic moments. The two iron ions then disproportionate at n/Fe > 0.375 to form ordered Fe^{2+}/Fe^{3+} mixed-valence dimers similar to the ones obtained in the AF structure at the same reduction rate. It should be noted here that when full structural relaxations are performed at each step of the reduction, the two iron ions disproportionate at a smaller reduction rate, *i.e.* at n/Fe > 0.25. Another interesting result concerns the relative energies of the AF and FM structures. Once electrons are added to the system, our calculations show that the energy difference between the FM and the AF structure almost vanishes. This is actually fully consistent with the significant dispersion of the redox band both along the inorganic chains and between the chains. As mentioned above, the filling of this band with electrons should favor some electronic delocalization in the system, and therefore the stabilization of the FM state with respect to the AF one.

To study the electrochemical reduction of the MIL53(Fe), lithium was added into the structure. A Connolly surface [25] was first computed to determine the different sites accessible for Li^+ ions. This algorithm uses a sphere of a particular radius for the solvent (here the Li^+ ion with a radius r = 1.0 Å) to probe the accessible surface area of the porous material. The result is shown in Fig. 5 and leads to four different sites. Site A lies close to the hydroxyl bridging ligand of the inorganic chains and favors a direct interaction between the Li^+ and the non-bonding electronic doublets of the hydroxyl group. Site B lies close to the carboxylic group of the BDC linkers and allows a direct interaction between Li^+ and the empty π-acceptor orbitals of the carboxylic group. Site C lies at the middle of the *c*-edge (0 0 1/2) or at the centre of the (*a*, *c*) face (1/2 0 1/2), both positions being crystallographically equivalent. This site allows a direct interaction of Li^+ with the two adjacent chains through the oxygen atoms of both hydroxyl and carboxylate groups. Eventually, site D lies in between two BDC and allows a direct interaction of Li^+ with the $\pi_\perp$-orbitals of the unsaturated benzene ring.

In Table 2 we have listed the A to D site energies obtained after full structural relaxations for two different lithium compositions for the AF structure, as well as the computed open-circuit voltages following the method reported in Ref. [21]. Note that for all calculations, the FM structure is closely related in energy to the AF one by at most 30 meV, suggesting that the magnetic interactions along

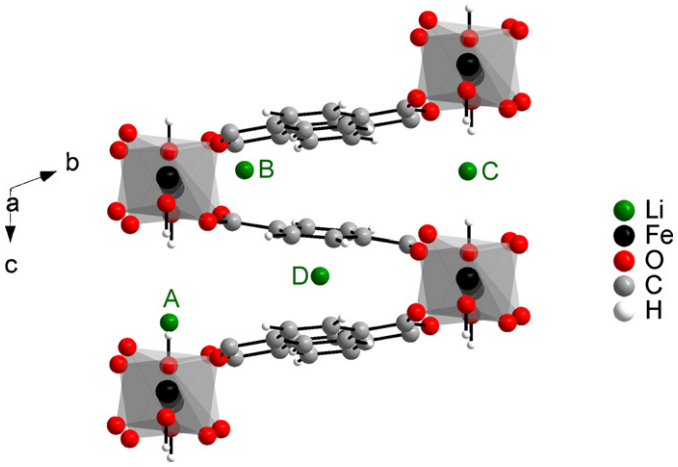

Fig. 5. Illustration of the four crystallographic sites A to D for lithium insertion (in green), as deduced from the Connolly surface of the MIL53(Fe). (For interpretation of the references to color in this figure legend, the reader is referred to the web version of the article.)

the chain are no longer sufficient to favor a long-range magnetic order in the lithiated compound. In order to reach the intermediate lithium composition xLi/Fe = 0.25, a $2 \times 1 \times 1$ super-cell consisting in 4 Fe per chain was built. The composition xLi/Fe = 0.5 was then computed within the same supercell to minimize the numerical errors associated with different unit-cell size calculations. The energy of site D was found 988 meV/Li above the other sites at xLi/Fe = 0.25 and was therefore ruled out from the study for xLi/Fe = 0.5. This energy is consistent with the very small interaction expected when a Li^+ interacts with a benzene ring through η^6-type coordination. Whatever the lithium composition considered, the A and B sites appear to be the most probable ones. The computed open-circuit voltages are also in better agreement with experiments for these two sites than for the others. As mentioned above, site A corresponds to the attack of the hydroxyl bridging ligand by a Li^+. This leads to the stabilization of a lithium hydroxide LiOH with a short Li–O bond distance equal to 1.88 Å and a Li–O–H angle of 123 for xLi = 0.25/Fe. Interestingly, Li(A) sits at nearly equivalent distances from the two iron ions as well as from the two O(BDC). This suggests an homogeneous reduction of Fe(1) and Fe(2) which is fully consistent with the stabilization of the FM structure compared to the AF one by 18 meV, and with the results of the electronic reduction. Site B corresponds to the attack of the carboxylic groups on the opposite side of the chain compared to site A. At xLi = 0.25/Fe, it leads to the stabilization of one short Li–O(BDC) and three longer ones, and the stabilization of a LiO_4 strongly distorted tetrahedron. In that case, Li(B) gets much closer to Fe(2) than to Fe(1) which results in a significant elongation of one Fe–O(BDC) bond (*i.e.* Fe(2)–O = 2.73 Å vs. Fe(1)–O = 1.97 Å). In this case, a preferential reduction of one every iron ion is obtained, in agreement with the electronic reduction for the AF state. Interestingly, when xLi/Fe is increased, site B becomes slightly favored compared to site A, leading to configurations 2B, 2A and A + B closely related

Table 2
Relative site energies Δ (meV/Li) for two different lithium compositions computed in the AF structure, the most stable site energy being set to zero, and open-circuit voltages $\bar{V}$ (in volts) computed from x = 0 to 0.25 and from x = 0.25 to 0.5. The calculations have been performed in the P_i unit cell in which the *a*-parameter (chain direction) has been doubled to reach the x = 0.25Li/Fe composition.

Li composition	xLi/Fe = 0.25				xLi = Fe 0.5						Exp.[a]
Li-sites filling	A	B	C	D	2A	2B	2C	A + B	A + C	B + C	
Δ (meV/Li) AFM	0	42	228	988	36	0	288	56	212	197	
$\bar{V}$(V)	2.76	2.73	2.47	–	2.55	2.74	2.40	2.63	2.47	2.49	2.8–2.6

[a] Ref. [5].

in energy at xLi/Fe = 0.5. Focusing on site C, the interaction of Li^+ with the oxygen atoms belonging to different chains induces a significant decrease of the *c* parameter due to the formation of two short Li–O(BDC) bonds of 1.94 Å and two longer ones of 2.58 Å for xLi = 0.25/Fe. When xLi is increased, this contraction is even more pronounced. This is actually not consistent with the experimental results for which *in situ* XRD collected upon the discharge (reduction) have clearly shown a significant enlargement of the pore-size. This pore breathing was attributed to the insertion into the pores of the organic molecules contained into the electrolyte of the electrochemical cell [5]. As a consequence, site C should not be favored in real electrochemical conditions.

4. Discussion

4.1. Reversible insertion mechanism from xLi/Fe = 0 to 0.5

The results presented in the previous section suggest that a solid solution should take place in the first part of the discharge. It would correspond to the stabilization of a delocalized electronic state along the chains induced by the insertion of lithium into site A which is thermodynamically favored. The local geometry of this site after a full structural relaxation at xLi/Fe = 0.25 is indeed perfectly consistent with the stabilization of a fractional $Fe^{(3-x/2)+}$ oxidation state for the metallic ions, and with the absence of any crystallographic discrimination of the Fe sites by *in situ* XRD. Although a partial occupancy of site B cannot be fully ruled out, it is likely that the energy difference between sites A and B at xLi/Fe = 0.25 is here sufficient to consider a majoritary lithium insertion into site A. From the electronic point of view, the delocalized state from reduction rates xLi/Fe = 0 to 0.25 could be understood as the stabilization of mixed-valence (MV) state of class III (or II) in the Robin and Day classification [26]. In the molecular picture, a mixed-valence dimer of class III is characterized by a low activation barrier between the two wheels corresponding to the two symmetrically related Fe^{2+}/Fe^{3+} and Fe^{3+}/Fe^{2+} localized states (see Fig. 6). This leads to fractional oxidation states for the two iron ions as well as equivalent crystallographic sites and local environments. This is in perfect agreement with experiments for which a solid solution process was clearly identified in the first part of the discharge using galvanostatic measurements and *in situ* XRD patterns [5].

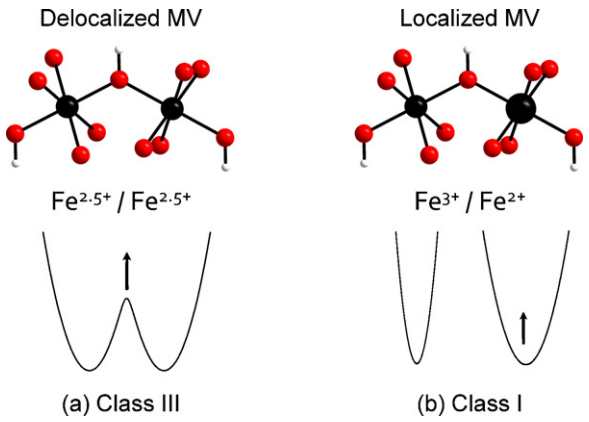

Fig. 6. Mixed-valence dimers of class III (a) and class I (b) following the Robin and Day classification. The Fe^{2+} ion is represented by a larger sphere than the Fe^{3+} one.

Above xLi/Fe = 0.25, our results suggest that a two-phase process takes place which corresponds to the stabilization of a localized electronic state along the chains. This state should be favored by a preferential lithium insertion into site B. Why this site is suddenly favored to site A is easy to understand using simple concepts of orbital and chemical bonding. As qualitatively shown in Fig. 7, the BDC ligand is a typical π-acceptor ligand with respect to Fe. In the molecular ionic picture, this means that one (at least) empty π-type orbital of the $(BDC)^{2-}$ lies above the occupied 3*d*-orbitals of the Fe^{3+} ion. When the symmetry of the system allows the BDC π-orbital(s) to interact with the metallic 3*d*-orbitals, then a more or less efficient metal to BDC back-donation mechanism takes place. The first consequence of this back-donation mechanism is to release some of the electron repulsions in the metallic 3*d*-orbitals, to stabilize the metallic-like antibonding orbitals with respect to a situation where

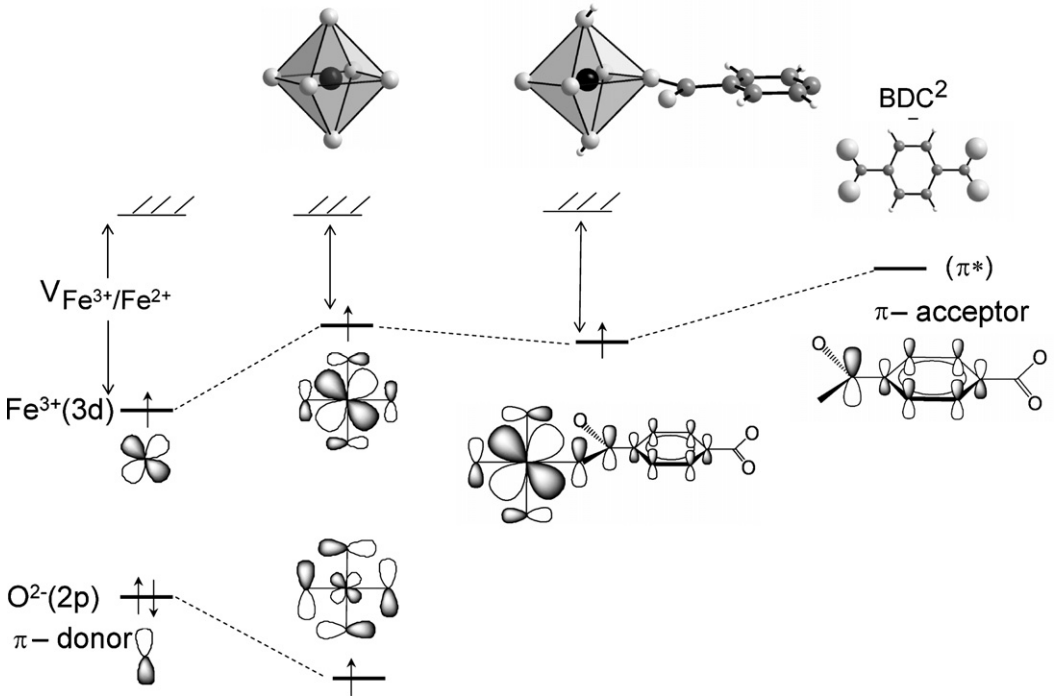

Fig. 7. Qualitative picture of the π-acceptor effects of a BDC^{2-} ligand on the molecular orbitals of the MO_6 octahedra.

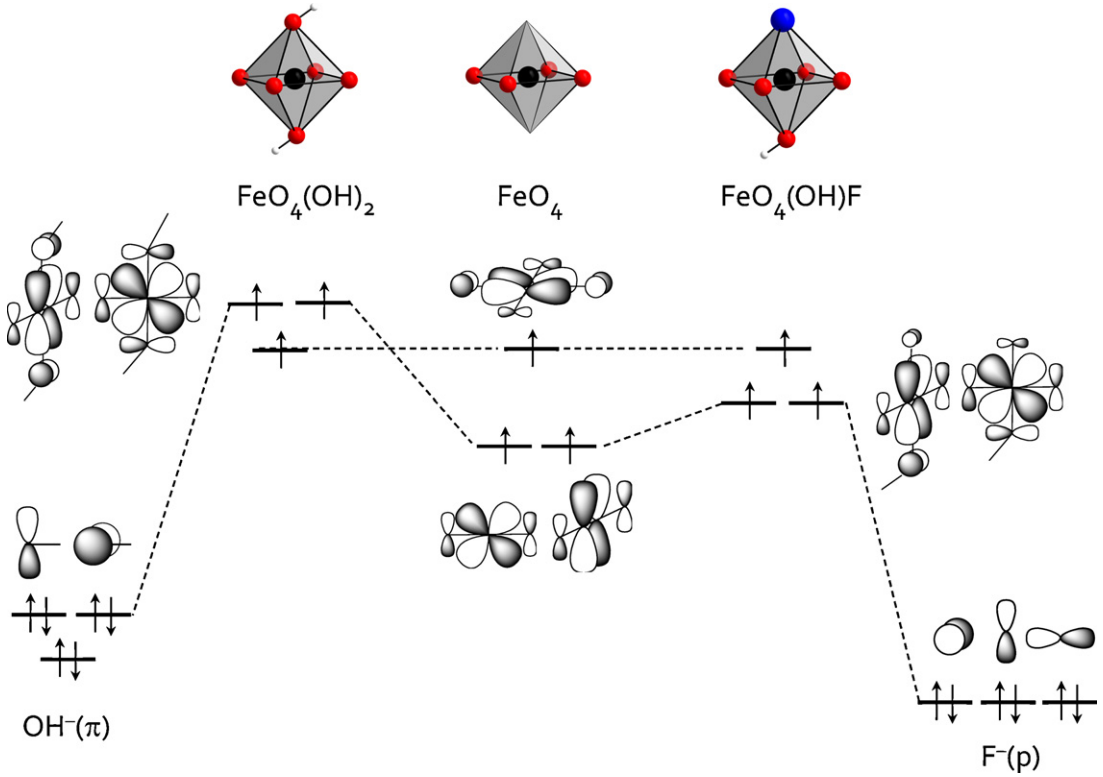

Fig. 8. Qualitative representation of the donor character of the OH^- and F^- ligands with respect to the transition metal and its consequence on the redox band of the fluorine-free and fluorinated MIL53(Fe) electrodes. The MO_4 fragment orbitals are used as the reference (middle) and two hydroxyl groups (left) or one hydroxyl group and one fluorine atom (right) are then added on the apical positions of the $MO_4(OH)_{2-x}F_x$ ($x = 0, 1$) final octahedron.

the transition metal would be surrounded by π-donor oxygen ligands (low-lying filled *p*-like orbitals lying below the 3*d*-metallic orbitals). In other words, the electrochemical potential for the Fe^{3+} to Fe^{2+} reduction is expected to be slightly higher in MIL53(Fe) than in iron oxides, as qualitatively depicted in Fig. 7. The second consequence of this back-donation mechanism is to increase the negative charge on the oxygen atoms of the carboxylic groups, and therefore to favor site B for a direct Li^+ attack with respect to site A. The filling of this site by lithium then results in a preferential reduction of one every iron ions (in a dimer representation) and in a significant distortion around the reduced Fe^{2+} which now adopts a pyramidal environment due to the partial breaking of one Fe–O(BDC) bond. A disproportionation reaction should thus take place along the chains above xLi/Fe = 0.25, leading to a progressive long-range ordering of mixed-valence Fe^{2+}/Fe^{3+} dimers of class I, in the Robin and Day classification [26] at xLi/Fe = 0.5. Compared to the MV states of class III (or II), the MV states of class I correspond to the localization of the extra-electron on one every iron and to crystallographic sites discrimination (see Fig. 6). This hypothesis is perfectly consistent with the appearance of a high-spin Fe^{2+} signal in the Mössbauer spectra of $Li_xMIL53(Fe)$ for lithium compositions xLi/Fe ≥ 0.3, and with the two-phase type evolution observed in the *in situ* XRD patterns above this reduction rate [5]. It also suggests that site B is responsible for the small capacity of the MIL53(Fe) electrode, since its filling provokes strong Fe–O bond destabilization and electron localization. It should be noted here that sites C and D cannot be reasonably considered as possible sites for lithium insertion. The filling of these sites not only leads to much higher energies per lithium than for sites A and B but also induces a significant contraction of the *c* parameter which is not consistent with the expansion characterized by *in situ* XRD upon discharge [5]. Looking at their crystallographic position (both standing in between two inorganic chains) it is easy to understand that the *c*-parameter contraction obtained in our calculations is the result of an artificial maximization of the Li^+–O(BDC) and Li^+–C(BDC) interactions for sites C and D, respectively.

4.2. Irreversible conversion mechanism from xLi/Fe = 0.5 to 1.0

The fact that lithium insertion is no longer possible above the composition xLi/Fe = 0.5, although available sites still exist in the structure, should be related to the particularly stable electronic ground state of the $Li_{0.5}$MIL53(Fe) composition with respect to that of higher compositions. To confirm this assumption, we have investigated further lithium insertion up to 1Li/Fe, by adding lithium into the most favorable A and B sites. Interestingly, we have successfully relaxed the $Li_{0.75}$MIL53(Fe) and LiMIL53(Fe) crystal structures, leading to a complete formal reduction of the remaining Fe^{3+} sites to Fe^{2+}. These structures are nevertheless characterized by strongly elongated Fe–O bonds and by much lower cohesive energy per atom compared to the structures obtained at xLi/Fe = 0, 0.25 and 0.5. This confirms that the local environment of the iron ions is strongly destabilized by the $Fe^{3+} \rightarrow Fe^{2+}$ reduction, as already shown for xLi/Fe = 0.25 and 0.5 when lithium inserts into site B. This confirms our hypothesis that site B is responsible for the small capacity of the MIL53(Fe) electrode. Its filling should lead to a dramatic loss of cohesive interactions between the inorganic chains and the organic linkers when more than half the Fe^{3+} ions are reduced to Fe^{2+} in the structure. The $Li_xMIL53(Fe)$ phases associated with lithium composition >xLi/Fe = 0.5 should therefore preferentially decompose above this composition, as it has been clearly demonstrated experimentally when the electrochemical cells were cycled down to 0.5 V in discharge [5].

4.3. Influence of the fluorine bridging ligand on the redox properties of MIL53(Fe)

Compared to the fluorine-free electrode, the $Fe(OH)_{1-y}F_y(BDC)$ containing a fraction of fluorine (y) show slightly improved capacities. Attempts to quantitatively correlate the reversible capacity of these electrodes to the y fluorine content had failed, but up to now the most promising electrochemical performance has been obtained for $y = 0.2$ in which up to ~0.6Li/Fe were successfully and reversible exchanged upon charge and discharge [5]. Note that no super-structures were detected in the XRD patterns of the fluorinated phases, suggesting a statistically distribution of F and OH along the chains. From a computational point of view, these disordered structures require large supercell calculations and become rapidly prohibitive. It is nevertheless possible to discuss the influence of the OH/F substitution on the redox properties of the $Fe(OH)_{1-y}F_y(BDC)$ electrodes, at least in a qualitative manner, using a simple orbital approach. As illustrated in Fig. 8, the strong electronegative character of fluorine makes the F^- ligand less donor (more negatively charged) than the oxygen of the OH^- group with respect to the transition metal. In other words, the F^- occupied $2p$-orbitals lie lower in energy than the OH^- π-orbitals so that the Fe($3d$)–F($2p$) antibonding interactions are less destabilizing than the Fe($3d$)–OH(π) ones. As a matter of fact, the redox properties of the fluorinated electrodes should be activated by the OH/F substitution due to the stabilization of the metallic $3d$-orbitals. Moreover, the electrochemical potential of the fluorinated electrodes is expected to be slightly increased compared to that of the fluorine-free electrode. Another interesting remark concerns the thermodynamic energies of site A and B. Recalling that the fluorine atoms locates along the chains as bridging ligands, it can be easily expected that site B (close to the BDC linkers) should not be affected by the y content, while site A should be as much favored as y increases. This suggests that the solid solution domain taking place in the first part of the discharge (filling of site A) should increase with the y fluorine content. Since our calculations show that lithium insertion into site B strongly destabilizes the fluorine-free electrode (ending the lithiation), it appears obvious that delaying its filling by enlarging the solid solution domain through OH/F substitutions will increase the reversible capacity of the resulting fluorinated electrodes.

5. Conclusion

The present study aims at elucidating the Li-induced redox mechanism of a complex MOF architecture. The use of DFT+U calculations coupled with chemical bond concepts and orbital analysis allowed us to fully interpret both the MIL53(Fe) ground state and its reactivity towards elemental lithium. This material is shown to be a weak antiferromagnetic charge transfer insulator at $T = 0$ K exhibiting a paramagnetic behavior at room temperature with iron ions in the high-spin $S = 5/2$ state. Its reactivity with respect to elemental lithium is the first evidence for a reversible lithium insertion reaction in such MOFs compounds. From experiments, the insertion reaction has been shown to proceed through a solid solution reaction followed by a two-phase reaction which ends around xLi/Fe = 0.5. This redox mechanism is here linked to the stabilization of a delocalized mixed-valence state of class III for the solid solution domain and a localized mixed-valence state of class I for the two-phase domain. The solid solution process is associated with lithium insertion into site A (close to the hydroxyl or fluorine bridging ligands along the chain), while the two-phase process corresponds to lithium insertion into site B (close to the BDC ligands). The two-phase process is shown to be at the origin of the small capacity of the MIL53(Fe) since its filling results in a strong destabilization of the inorganic/organic interactions responsible for the cohesion of the MIL53(Fe) framework. Above the critical composition xLi/Fe = 0.5, our computations suggest that an irreversible decomposition of the electrode should take place, whose driving force is a complete loss of the cohesive interactions between the inorganic and organic networks of the MOFs architecture.

Acknowledgments

This work has been financially supported by the "Agence Nationale de le Recherche" (ANR) through the project ANR-06-0202 CONDMOF and by the French national resources centers IDRIS and CINES. The authors thank J.-M. Tarascon and G. Férey for sharing their experimental results and fruitful discussions.

References

[1] A.K. Padhi, K.S. Nanjundaswamy, J.B. Goodenough, J. Electrochem. Soc. 144 (1997) 1188.
[2] A.K. Padhi, K.S. Nanjundaswamy, C. Masquelier, S. Okada, J.B. Goodenough, J. Electrochem. Soc. 144 (1997) 1609.
[3] A.K. Padhi, K.S. Nanjundaswamy, C. Masquelier, J.B. Goodenough, J. Electrochem. Soc. 144 (1997) 2581.
[4] C. Combelles, M. Ben Yahia, L. Pedesseau, M.-L. Doublet, J. Phys. Chem. C 114 (2010) 9518.
[5] G. Férey, F. Millange, M. Morcrette, C. Serre, M.-L. Doublet, J.M. Grenèche, J.-M. Tarascon, Angew. Chem. Int. Ed. 46 (2007) 3259.
[6] S.T. Wilson, B.M. Lok, C.A. Messina, T.R. Cannan, E.M. Flanigen, J. Am. Chem. Soc. 104 (1982) 1146.
[7] A.K. Cheetham, G. Férey, T. Loiseau, Angew. Chem. 111 (1999) 3466; A.K. Cheetham, G. Férey, T. Loiseau, Angew. Chem. Int. Ed. 38 (1999) 3269.
[8] K. Seki, W. Mori, J. Phys. Chem. B 106 (2002) 1380.
[9] S. Bourrelly, P.L. Llewellyn, C. Serre, F. Millange, T. Loiseau, G. Férey, J. Am. Chem. Soc. 1271 (2005) 3519.
[10] N.L. Rosi, J. Eckert, M. Eddaoudi, D.T. Vodak, J. Kim, M.O.S. Keeffe, O.M. Yaghi, Science 300 (2003) 1127.
[11] G. Férey, M. Latroche, C. Serre, F. Millange, T. Loiseau, A. Percheron-Guegan, Chem. Commun. (2003) 2976.
[12] X.B. Zhao, B. Xiao, A.J. Fletcher, K.M. Thomas, D. Bradshaw, M.J. Rosseinsky, Science 306 (2004) 1012.
[13] V.I. Anisimov, J. Zaanen, O.K. Andersen, Phys. Rev. B 44 (1991) 943.
[14] A.I. Liechtenstein, V.I. Anisimov, J. Zaanen, Phys. Rev. B 52 (1995) R5467.
[15] S.L. Dudarev, G.A. Botton, S.Y. Savrasov, C.J. Humphreys, A.P. Sutton, Phys. Rev. B 57 (1998) 1505.
[16] J.P. Perdew, A. Zunger, Phys. Rev. B 23 (1981) 5048.
[17] C. Combelles, M.-L. Doublet, Ionics 14 (2008) 279.
[18] G. Kresse, J. Hafner, Phys. Rev. B 47 (1993) 558.
[19] G. Kresse, J. Furthmuller, Comput. Mater. Sci. 6 (1996) 15.
[20] J.P. Perdew, K. Burke, M. Ernzerhof, Phys. Rev. Lett. 77 (1996) 3865.
[21] F. Zhou, M. Cococcioni, C.A. Marianetti, D. Morgan, G. Ceder, Phys. Rev. B 70 (2004) 235121.
[22] G. Kresse, D. Joubert, Phys. Rev. B 59 (1999) 1758.
[23] B. Dorado, B. Amadon, M. Freyss, M. Bertolus, Phys. Rev. B 79 (2009) 235125.
[24] J.M. Tarascon, G. Férey, private communication.
[25] M.-L. Connolly, Science 221 (1983) 709.
[26] M.B. Robin, P. Day, Adv. Inorg. Chem. Radiochem. 10 (1967) 247.